NEUROINFLAMMATION

C9orf72 is required for proper macrophage and microglial function in mice

J. G. O'Rourke,[1] L. Bogdanik,[2] A. Yáñez,[1] D. Lall,[1] A. J. Wolf,[3] A. K. M. G. Muhammad,[1] R. Ho,[1] S. Carmona,[1] J.P. Vit,[3] J. Zarrow,[1] K. J. Kim,[1] S. Bell,[1] M. B. Harms,[5] T. M. Miller,[5] C. A. Dangler,[2] D. M. Underhill,[3] H. S. Goodridge,[1] C. M. Lutz,[2] R. H. Baloh[1,4]*

Expansions of a hexanucleotide repeat (GGGGCC) in the noncoding region of the *C9orf72* gene are the most common genetic cause of amyotrophic lateral sclerosis (ALS) and frontotemporal dementia. Decreased expression of *C9orf72* is seen in expansion carriers, suggesting that loss of function may play a role in disease. We found that two independent mouse lines lacking the *C9orf72* ortholog (*3110043O21Rik*) in all tissues developed normally and aged without motor neuron disease. Instead, *C9orf72* null mice developed progressive splenomegaly and lymphadenopathy with accumulation of engorged macrophage-like cells. *C9orf72* expression was highest in myeloid cells, and the loss of *C9orf72* led to lysosomal accumulation and altered immune responses in macrophages and microglia, with age-related neuroinflammation similar to *C9orf72* ALS but not sporadic ALS human patient tissue. Thus, *C9orf72* is required for the normal function of myeloid cells, and altered microglial function may contribute to neurodegeneration in *C9orf72* expansion carriers.

Amyotrophic lateral sclerosis (ALS) and frontotemporal dementia (FTD) are neurodegenerative disorders with overlapping clinical presentations, pathology, and genetic origins (*1*, *2*). Expansions of a GGGGCC hexanucleotide repeat in the first intron/promoter of the *C9orf72* gene are the most commonly identified genetic cause of ALS/FTD (*3*, *4*) and are found in other neurodegenerative diseases (*5*). Microglial dysfunction is strongly tied to ALS/FTD pathogenesis (*6*), with mutations in progranulin causing FTD (*7*, *8*) and variants in the microglial expressed genes *TREM2* and *TBK1* implicated in ALS (*9*–*11*). However, no connection has been made between microglial function and *C9orf72*, where focus instead has been on its role in neurons (*12*, *13*). Although the repeat expansion leads to decreased *C9orf72* expression in human patient tissues, most research has focused on gain-of-function toxicity as the primary mechanism in disease rather than loss of function (*14*–*18*).

To investigate the function of the mouse ortholog of *C9orf72* (*3110043O21Rik*, referred to as *C9orf72* below), we analyzed two independent loss-of-function alleles in mice (figs. S1 and S2). *C9orf72*$^{+/-}$ and *C9orf72*$^{-/-}$ mice showed normal weight gain and life span; had normal sensorimotor coordination, limb strength, femoral motor and sensory axon counts, and muscle electrophysiology; and showed no evidence of neurodegeneration on histology through advanced age (17 months) (figs. S1 to S3). The only histologic abnormalities in the nervous system were rare chromatolytic structures seen with hemotoxylin and eosin (H&E) staining, found in both gray and white matter of the spinal cord, that did not increase with age or show reactive gliosis (fig. S3). All studies were performed using the Knockout Mouse Project line except where specified.

C9orf72$^{-/-}$ mice from both lines developed visibly enlarged cervical lymph nodes and spleens (Fig. 1, A and B), detectable as early as 1 month after birth, that slowly enlarged with age (Fig. 1C and fig. S2). No gross or histological defects were observed in other organs at 5 months of age. Histology of lymph nodes and the white pulp of the spleen showed disruption of the normal follicular structure by enlarged debris-filled cells (Fig. 1D) that expressed CD11b and contained ubiquitin- and p62-positive vacuoles consistent with macrophages (Fig. 2A and fig. S4). Immunoblotting confirmed increased amounts of p62 and LC3 proteins, indicating an increase in components of the autophagy machinery in homozygote spleens (Fig. 2B). Massive up-regulation of *Trem2* expression was observed in *C9orf72*$^{-/-}$ spleens, a cell surface receptor expressed by macrophages and monocytes, as were inflammatory cytokines, including IL-1β, IL-6, and IL-10 (Fig. 2C). Despite the altered follicular architecture, there were no differences in the proportions of B cells, T cells, or CD11b^{+} myeloid cells (Fig. 2D and fig. S2J). However, flow cytometry revealed changes in myeloid subsets, including the emergence of a CD11b^{+}Ly6C^{-}Ly6G^{int} population unique to *C9orf72*$^{-/-}$ mice, and a decrease in F4/80^{+} red pulp macrophages, indicating that *C9orf72* deficiency has a selective effect on myeloid populations in the spleen (Fig. 2, E to G). Complete blood counts and flow cytometry of bone marrow were normal in *C9orf72*$^{-/-}$ mice at 5 months (fig. S5), supporting the idea that splenic enlargement was not related to deficient hematopoiesis in bone marrow.

Given the progressive splenomegaly with altered myeloid cells, and the buildup of engorged macrophages with accumulations of LC3 and p62 in the spleens of *C9orf72*$^{-/-}$ mice, we hypothesized that C9orf72 protein is important for endosomal trafficking in macrophages. We first examined the expression of *C9orf72* by fluorescence-activated cell sorting (FACS) of different populations from wild-type mouse spleens and found that *C9orf72* was expressed at high levels in CD11b^{+} (myeloid cell), as compared to CD3^{+} (T cell) and CD19^{+} (B cell) populations (Fig. 3A). Query of the immunological genome project (www.immgen.org) confirmed that the expression of *C9orf72* was highest in macrophages and dendritic cells as compared to other immune cells (fig. S6, A and B). Pathway analysis (*19*) of the 35 genes in the *C9orf72* constellation was significant for only one pathway, lysosomal function (Bonferroni $P = 2.32^{-6}$) (fig. S6C). To examine whether *C9orf72* is necessary for macrophage function, we differentiated bone marrow–derived macrophages (BMDMs) from *C9orf72*$^{-/-}$ mice and stained them for endosomal markers. BMDMs from *C9orf72*$^{-/-}$ mice showed marked accumulation of LysoTracker- and Lamp1-positive vesicles, indicating a defect in late endosome/lysosomal trafficking (Fig. 3, B and C). No changes in the early or late endosomal markers Rab5 or Rab7 were observed (figs. S7 and S8). The accumulation of LysoTracker- and Lamp1-positive vesicles was rescued by viral expression of human *C9orf72*, indicating that this defect was due to the loss of *C9orf72* (Fig. 3, D and E). *C9orf72*$^{-/-}$ BMDMs showed normal initial phagocytosis of zymosan particles (Fig. 3F); however, BMDMs from both *C9orf72*$^{-/-}$ and to a lesser extent *C9orf72*$^{+/-}$ mice showed enhanced production of phagocyte oxidase-derived reactive oxygen species (ROS) after feeding with zymosan particles (Fig. 3G), which has been reported in cells with defective fusion of phagosomes to lysosomes (*20*). BMDMs from *C9orf72*$^{-/-}$ and *C9orf72*$^{+/-}$ mice also showed enhanced cytokine production in response to several immune stimuli, including those sensed in endosomal/lysosomal compartments such as peptidoglycan, CpG, and silica (Fig. 3, H and I). Thus, *C9orf72* is critical for the proper function of macrophages, and the loss of *C9orf72* leads to a pro-inflammatory state that probably drives the splenic and lymph node hyperplasia. Although hemizygous mice did not have a phenotype at the tissue level, haploinsufficiency of *C9orf72* led to altered inflammatory responses in macrophages at the cellular level, which could lead to a physiological phenotype when the system is stressed.

[1]Board of Governors Regenerative Medicine Institute, Cedars-Sinai Medical Center, 8700 Beverly Boulevard, Los Angeles, CA 90048, USA. [2]The Jackson Laboratory, Bar Harbor, ME, USA. [3]Division of Biomedical Sciences, Cedars-Sinai Medical Center, 8700 Beverly Boulevard, Los Angeles, CA 90048, USA. [4]Department of Neurology, Cedars-Sinai Medical Center, 8700 Beverly Boulevard, Los Angeles, CA 90048, USA. [5]Department of Neurology, Washington University School of Medicine, 660 South Euclid Avenue, St. Louis, MO 63110, USA.
*Corresponding author. E-mail: robert.baloh@csmc.edu

The defects in *C9orf72*$^{-/-}$ BMDMs raised the possibility that other myeloid cells, including resident microglia in the brain, also require *C9orf72* for normal function. Although an earlier report suggested that microglia express low levels of *C9orf72* (*12*), we observed that microglia showed the highest levels of *C9orf72* expression of any cell type in the brain in published data sets (*21*–*23*) (Fig. 3J) and in quantitative reverse transcription polymerase chain reaction (qRT-PCR) of cells isolated from adult mouse brains (Fig. 3K). Microglia from *C9orf72*$^{-/-}$ mice showed accumulation of LysoTracker- and Lamp1-positive structures, similar to BMDMs (Fig. 3, L and M), whereas primary cortical neurons did not (fig. S9). To probe the functional state of microglia lacking *C9orf72*, we performed qRT-PCR on spinal cord microglia isolated from *C9orf72*$^{-/-}$ mice and found increased levels of cytokines IL-6 and IL-1b, supporting the idea that the altered lysosomal function leads to a proinflammatory state (Fig. 4A) similar to that observed in BMDMs.

Although we did not see overt neurodegeneration in *C9orf72*$^{-/-}$ mice, given the pro-inflammatory phenotype in isolated microglia, we used transcriptional profiling to investigate *C9orf72*-deficient nervous tissue in greater detail. Gene set enrichment analysis (GSEA) on RNA sequencing (RNA-seq) of spinal cords from young animals (3 months) showed little difference between genotypes. In contrast, in aged animals (17 months), a large number of pathways were altered in *C9orf72*$^{-/-}$ versus *C9orf72*$^{+/-}$ or wild-type animals [false discovery rate (FDR) < 0.05] (Fig. 4B). We focused on the 19 pathways that were up-regulated in *C9orf72*$^{-/-}$ versus *C9orf72*$^{+/-}$ and control animals for further analysis (fig. S10). Of these 19 pathways, almost a third [6 out of 19 (6/19)] were related to inflammation (Fig. 4C). To determine whether similar changes are observed in *C9orf72* ALS (C9-ALS) tissue, we analyzed a recent RNA-seq data set that includes normal controls, sporadic ALS (sALS), and C9-ALS cases (*24*). Of the 19 up-regulated pathways in *C9orf72*$^{-/-}$ mice, there was little overlap (1/19) with pathways up-regulated in sporadic ALS brain tissue (frontal cortex or cerebellum; Fig. 4D). In contrast, the majority (10/19) of pathways up-regulated in *C9orf72*$^{-/-}$ mice were also up-regulated in C9-ALS human patient brains, including nearly all of the immune pathways (5/6). A direct comparison showed a significant increase in inflammatory pathways in C9-ALS versus sALS cases (fig. S11). Finally, we performed immunostaining for Iba1 and Lamp1 on motor cortex and spinal cord tissue from C9-ALS (n = 3) and sALS (n = 3) cases. Although frequent reactive microglia were present in all ALS cases, microglia containing large accumulations of Lamp1-positive material were only observed in the C9-ALS cases (Fig. 4E and fig. S11). Thus, both transcriptome and histologic analyses of C9-ALS patient tissue are consistent with the idea that the decreased *C9orf72* expression in C9-ALS leads to altered microglial function and neuroinflammation.

In summary, the loss of *C9orf72* in mice led to age-related inflammation in the spleen and

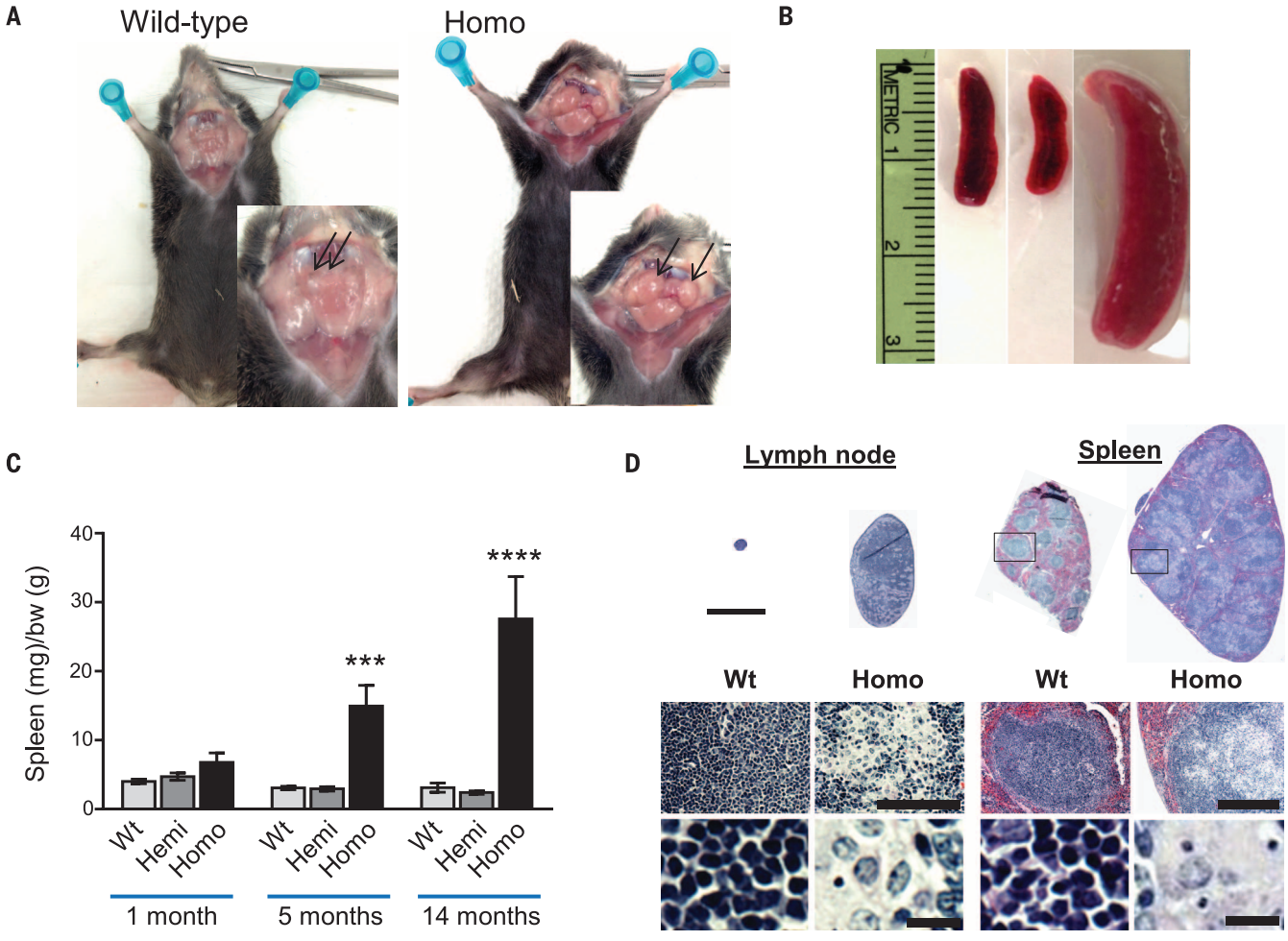

Fig. 1. Generation of *C9orf72* (*3110043O21Rik*) null mice. (**A**) Gross images of cervical lymphadenopathy (arrows) in *C9orf72*$^{-/-}$ mice (9 months of age). Wt, wild-type; homo, homozygote. (**B**) Gross images of splenomegaly (12 months of age). (**C**) Spleen weights (in milligrams) normalized to body weight (in grams) at indicated ages [***P = 0.0008, ****P < 0.0001, two-way analysis of variance (ANOVA)]. (**D**) H&E staining of wild-type and homozygote lymph nodes and spleens at 5 months (top; scale bar = 3 mm) showing disruption of follicular architecture in null mice by large cells with swollen cytoplasm. Higher-magnification images shown in bottom panels; scale bars = 100 μm and 10 μm (lymph node) and 300 μm and 10 μm (spleen).

nervous system, with defects in lysosomal trafficking and immune responses in macrophages and microglia. The disruption of lysosomal function in macrophages is consistent with the idea that *C9orf72* is a member of the DENN family of Rab-GEFs involved in late endosomal trafficking and autophagy (*25*–*27*). Our data support a model where *C9orf72* regulates the maturation of phagosomes to lysosomes in macrophages, because we observed both altered responses to immune stimuli, including those sensed in endosomal/lysosomal compartments (PGN, CpG, and silica) in BMDMs lacking *C9orf72*. Furthermore, loss of *C9orf72* function could affect neurodegeneration in C9-ALS and FTD by diminishing the ability of microglia to clear aggregated proteins and/or altering their immune responses. Our findings of altered immune responses in haploinsufficient macrophages indicate that even this partial decrease in *C9orf72* levels could affect microglial function (*3*, *28*–*30*). These data raise the possibility of a dual-effect mechanism for the pathogenesis of a single gene defect: that gain-of-function manifestations of *C9orf72* expansion (RNA foci and RAN dipeptides) in neurons are coupled with "primed" and dysfunctional microglia, which ultimately results in neurodegeneration (*31*). Given that many ALS genes are involved in late endosomal trafficking and lysosome function (*TBK1*, *TMEM106B*, *OPTN*, *SQSTM1*, *UBQLN2*, *VCP*, *CHMP2B*, and *PGRN*) (*32*) and are expressed in both neurons and microglia, the concept of a dual-effect mechanism may generalize to other forms of inherited ALS.

Finally, our findings raise important considerations about therapeutic knockdown of *C9orf72* in the nervous system. Although these approaches effectively target gain-of-function manifestations in neurons, they could exacerbate microglial dysfunction by further suppressing *C9orf72*, unless they specifically target repeat-containing transcripts (*33*). An initial report of *C9orf72* knockdown in

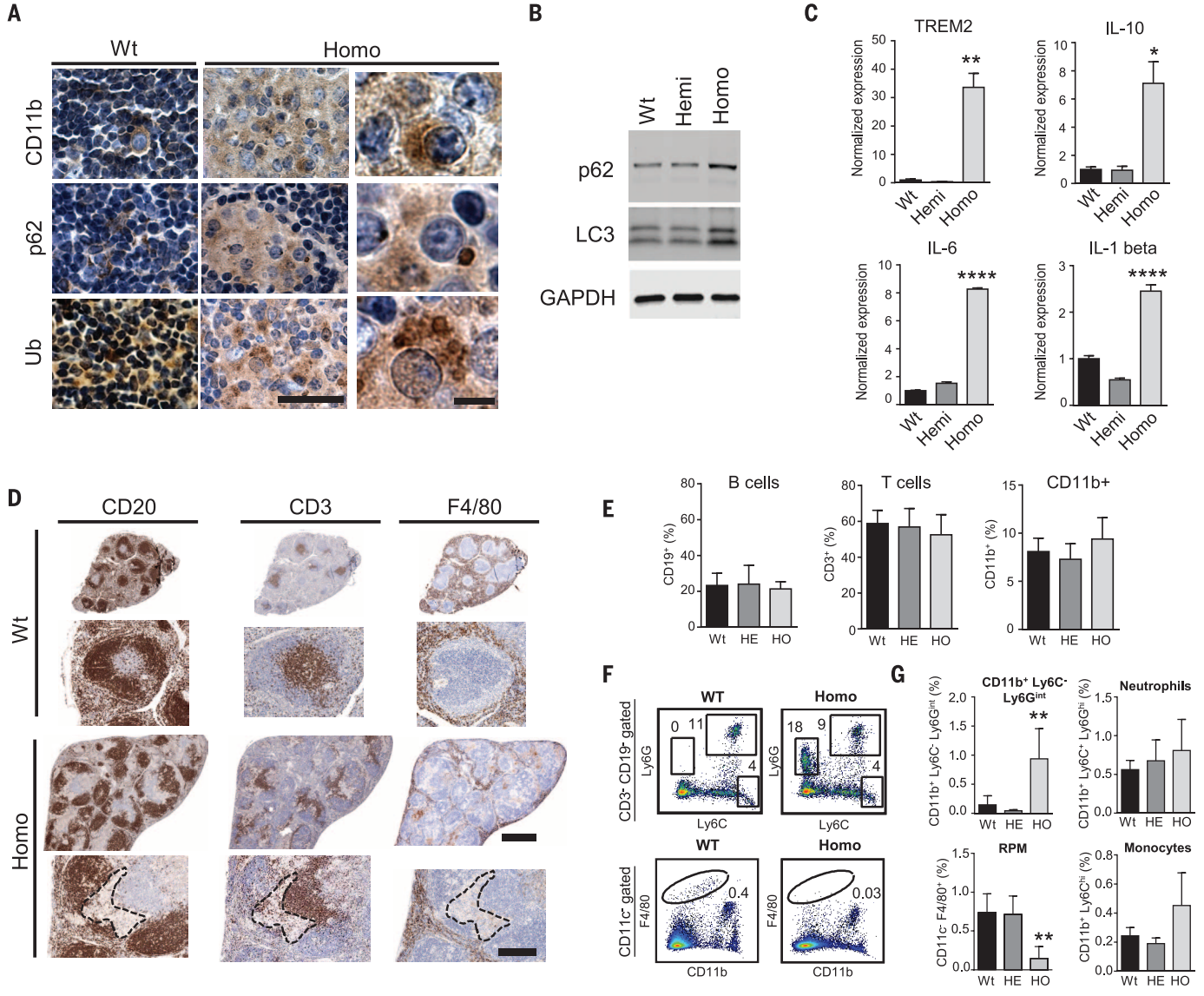

Fig. 2. *C9orf72* null mice develop progressive splenomegaly with engorged macrophages, altered monocyte populations, and inflammation. (**A**) Enlarged cells in homozygote spleens (5 months) stained for CD11b and containing p62 and ubiquitin (Ub) accumulations. Scale bars = 100 μm and 20 μm. (**B**) Immunoblot of spleen lysates showed an increase in p62 and LC3 in *C9orf72*$^{-/-}$ mice (n = 3; 14 months). (**C**) qRT-PCR analysis of spleens (14 months) showed an increase in macrophage marker *Trem2* (**P = 0.008), and cytokines IL-10 (*P = 0.035), IL-6 (****P < 0.0001), and IL-1β (****P < 0.0001; one-way ANOVA). (**D**) Immunostains of wild-type and *C9orf72*$^{-/-}$ spleens (5 months) for CD20 (B cells), CD3 (T cells), and F4/80 (red pulp macrophages). The dashed outline highlights the region of abnormal CD11b^{+} cells in the *C9orf72*$^{-/-}$ spleens. Scale bars = 1 mm and 300 μm. (**E**) FACS analysis of spleens (5 months). (**F**) Dot plots and (**G**) bar graphs showed a unique population of CD11b^{+} Ly6C^{-}Ly6G^{int} cells in *C9orf72*$^{-/-}$ spleens and a decrease in F4/80^{+} red pulp macrophages as compared to wild-type mice or hemizygotes (n = 4; 5 months) (**P = 0.01, one-way ANOVA).

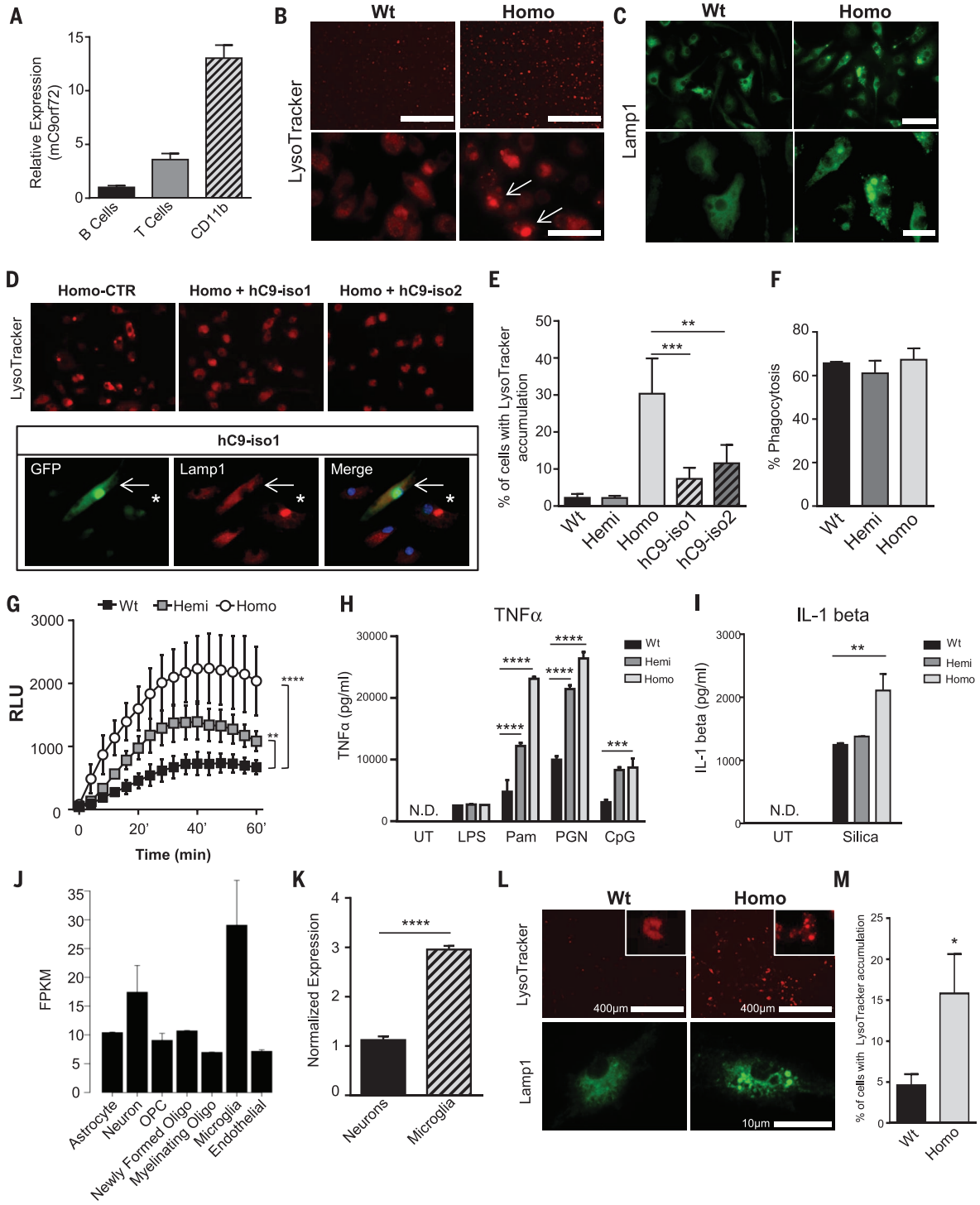

Fig. 3. Analysis of macrophages and microglia from *C9orf72*-deficient mice. (**A**) qRT-PCR analysis from B cells, T cells, and CD11b^{+} cells FAC-sorted from wild-type mouse spleens (n = 2). (**B** and **C**) BMDMs from *C9orf72*$^{-/-}$ mice showed accumulation of LysoTracker- and Lamp1-stained vesicles as compared to wild-type mice. Scale bars = 50 μm and 20 μm. (**D**) *C9orf72*$^{-/-}$ BMDMs treated with lentivirus encoding either human C9orf72 isoform 1-IRES-GFP (hC9-iso1) or isoform 2-IRES-GFP (hC9-iso2). LysoTracker (top panel) or Lamp1 (bottom panel) accumulation was rescued by either hC9-iso1 or hC9-iso2 (top panel). Arrow, hC9-iso1 infected cell; asterisk, uninfected cell. (**E**) Quantitation of LysoTracker accumulation in BMDMs of the indicated genotype or homozygotes treated with hC9-iso1 and hC9-iso2 lentivirus (***P = 0.0002, **P = 0.0018, one-way ANOVA). (**F**) BMDMs fed with fluorescent zymosan particles for 15 min and then analyzed by FACS analysis. (**G**) ROS production by BMDMs after zymosan ingestion in indicated genotypes (****P = <0.0001, two-way ANOVA). (**H**) *C9orf72*$^{+/-}$ and *C9orf72*$^{-/-}$ BMDMs showed increased TNF-α production after stimulation with Pam_3CSK_4 (Pam), peptidoglycan (PGN), and CpG, but not lipopolysaccharide (LPS) (****P < 0.0001, ***P = 0.0002, two-way ANOVA; N.D., not detected). (**I**) IL-1β production after stimulation with silica (*P < 0.05, two-way ANOVA). (**J**) RNA-seq of *C9orf72* in indicated cell types from the cerebral cortex (*21*). (**K**) qRT-PCR of *C9orf72* from neurons and microglia isolated from the adult mouse brain. (**L**) Microglia purified from *C9orf72*$^{-/-}$ mice showed accumulation of LysoTracker- and Lamp1-positive enlarged vesicles. (**M**) Quantification of percentage of microglia with enlarged LysoTracker-positive vesicles (*P = 0.027, one-tailed t test).

A

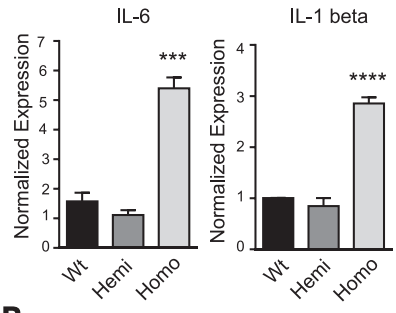

B

UP
DOWN

3 months			
	Wt	Hemi	Homo
Wt		0	7
Hemi	0		9
Homo	0	1	

17 months			
	Wt	Hemi	Homo
Wt		0	28
Hemi	9		103
Homo	13	38	

C

	Pathway	FDR q-value (Homo vs Wt)
Inflammation		
1	REACTOME_INTERFERON_GAMMA_SIGNALING	0.013555
2	REACTOME_ER_PHAGOSOME_PATHWAY	0.019014
3	REACTOME_INTERFERON_ALPHA_BETA_SIGNALING	0.020657
4	KEGG_COMPLEMENT_AND_COAGULATION_CASCADES	0.021579
5	REACTOME_ANTIGEN_PROCESSING_CROSS_PRESENTATION	0.022685
6	REACTOME_CELL_SURFACE_INTERACTIONS_AT_THE_VASCULAR_WALL	0.044707
Ribosome and amino acid metabolism		
7	REACTOME_REGULATION_OF_ORNITHINE_DECARBOXYLASE_ODC	0.018841
8	REACTOME_AMINO_ACID_AND_OLIGOPEPTIDE_SLC_TRANSPORTERS	0.019372
9	REACTOME_SRP_DEPENDENT_COTRANSLATIONAL_PROTEIN_TARGETING_TO_MEMBRANE	0.023572
10	KEGG_RIBOSOME	0.025481
11	STRUCTURAL_CONSTITUENT_OF_RIBOSOME	0.02626
12	REACTOME_METABOLISM_OF_AMINO_ACIDS_AND_DERIVATIVES	0.027797
Cell cycle		
13	REACTOME_CYCLIN_E_ASSOCIATED_EVENTS_DURING_G1_S_TRANSITION	0.019978
14	REACTOME_SCFSKP2_MEDIATED_DEGRADATION_OF_P27_P21	0.038089
Cytochrome P450 metabolism		
15	KEGG_METABOLISM_OF_XENOBIOTICS_BY_CYTOCHROME_P450	0.023326
16	KEGG_DRUG_METABOLISM_CYTOCHROME_P450	0.025163
Glycoprotein biosynthesis		
17	KEGG_N_GLYCAN_BIOSYNTHESIS	0.023445
18	NABA_ECM_GLYCOPROTEINS	0.028687
19	REACTOME_BIOSYNTHESIS_OF_THE_N_GLYCAN_PRECURSOR_DOLICHOL_LIPID_LINKED_OLIGOSACCHARIDE_LLO_AND_TRANSFER_TO_A_NASCENT_PROTEIN	0.029621

D

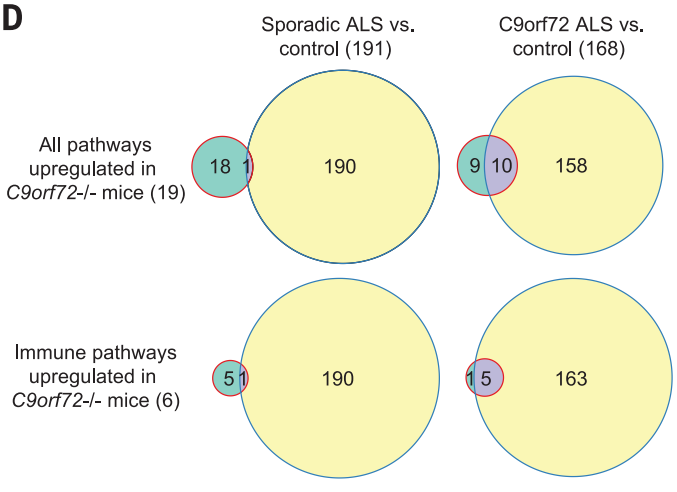

E

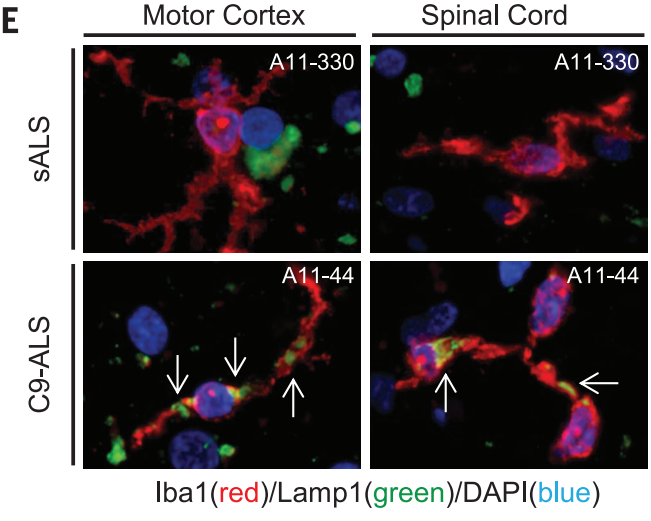

Fig. 4. Neuroinflammation in *C9orf72*$^{-/-}$ mice and *C9orf72* expansion human patient tissue. (**A**) qRT-PCR of inflammatory cytokines (IL-6 and IL-1β) in microglia isolated from *C9orf72*$^{-/-}$ mice (***P = 0.0007; **** P = <0.0001, one-way ANOVA). (**B**) Tables showing the number of up- and down-regulated pathways on GSEA (FDR < 0.05) of RNA-seq from 3- and 17-month-old lumbar spinal cords. (**C**) Table of up-regulated pathways in *C9orf72*$^{-/-}$ versus *C9orf72*$^{+/-}$ and wild-type mouse spinal cords (FDR < 0.05) at 17 months. Pathways up-regulated in both *C9orf72*$^{-/-}$ mice and human C9-ALS brain tissue are highlighted in red. (**D**) (Top) Venn diagrams showing overlap between the 19 up-regulated pathways in *C9orf72*$^{-/-}$ mice from (C) and those up-regulated in the cortex or cerebellum of sporadic ALS (left) or *C9orf72* ALS (right). (Bottom) Venn diagrams for the immune pathways from (C). (**E**) Human motor cortex and spinal cord tissue from C9-ALS and sALS cases double-labeled with Iba1 (red) to identify microglia and Lamp1 (green). Large accumulations of Lamp1 immunoreactivity (white arrows) were detected in activated microglia of C9-ALS but not sALS tissue.

mice using ASOs revealed up-regulation of immune markers in the nervous system, including *Trem2* and *Tyrobp* (*34*), suggesting that innate immune function should be monitored when performing *C9orf72* knockdown strategies in humans.

REFERENCES AND NOTES

1. C. Lomen-Hoerth, T. Anderson, B. Miller, *Neurology* **59**, 1077–1079 (2002).
2. A. S. Chen-Plotkin, V. M. Lee, J. Q. Trojanowski, *Nat Rev Neurol* **6**, 211–220 (2010).
3. M. DeJesus-Hernandez *et al.*, *Neuron* **72**, 245–256 (2011).
4. A. E. Renton *et al.*, *Neuron* **72**, 257–268 (2011).
5. J. Cooper-Knock, P. J. Shaw, J. Kirby, *Acta Neuropathol.* **127**, 333–345 (2014).
6. K. G. Hooten, D. R. Beers, W. Zhao, S. H. Appel, *Neurotherapeutics* **12**, 364–375 (2015).
7. M. Baker *et al.*, *Nature* **442**, 916–919 (2006).
8. M. Cruts *et al.*, *Nature* **442**, 920–924 (2006).

9. J. Cady *et al.*, *J. Am. Med. Assoc. Neurol.* **71**, 449 (2014).
10. E. T. Cirulli *et al.*, *Science* **347**, 1436–1441 (2015).
11. A. Freischmidt *et al.*, *Nat. Neurosci.* **18**, 631–636 (2015).
12. N. Suzuki *et al.*, *Nat. Neurosci.* **16**, 1725–1727 (2013).
13. M. Koppers *et al.*, *Ann. Neurol.* **78**, 426–438 (2015).
14. P. Fratta *et al.*, *Acta Neuropathol.* **126**, 401–409 (2013).
15. S. Mizielinska, A. M. Isaacs, *Curr. Opin. Neurol.* **27**, 515–523 (2014).
16. K. Zhang *et al.*, *Nature* **525**, 56–61 (2015).
17. B. D. Freibaum *et al.*, *Nature* **525**, 129–133 (2015).
18. A. Jovičić *et al.*, *Nat. Neurosci.* **18**, 1226–1229 (2015).
19. W. Huang, B. T. Sherman, R. A. Lempicki, *Nat. Protoc.* **4**, 44–57 (2009).
20. J. Ma, C. Becker, C. Reyes, D. M. Underhill, *J. Immunol.* **192**, 1356–1360 (2014).
21. Y. Zhang *et al.*, *J. Neurosci.* **34**, 11929–11947 (2014).
22. K. Sharma *et al.*, *Nat. Neurosci.* **18**, 1819–1831 (2015).
23. O. Butovsky *et al.*, *Nat. Neurosci.* **17**, 131–143 (2014).
24. M. Prudencio *et al.*, *Nat. Neurosci.* **18**, 1175–1182 (2015).
25. D. Zhang, L. M. Iyer, F. He, L. Aravind, *Front. Genet.* **3**, 283 (2012).
26. T. P. Levine, R. D. Daniels, A. T. Gatta, L. H. Wong, M. J. Hayes, *Bioinformatics* **29**, 499–503 (2013).
27. M. A. Farg *et al.*, *Hum. Mol. Genet.* **23**, 3579–3595 (2014).
28. Z. Xi *et al.*, *Am. J. Hum. Genet.* **92**, 981–989 (2013).
29. V. V. Belzil *et al.*, *Acta Neuropathol.* **126**, 895–905 (2013).
30. J. Russ *et al.*, *Acta Neuropathol.* **129**, 39–52 (2015).
31. V. H. Perry, C. Holmes, *Nat. Rev. Neurol.* **10**, 217–224 (2014).
32. O. M. Peters, M. Ghasemi, R. H. Brown Jr., *J. Clin. Invest.* **125**, 2548 (2015).
33. D. Sareen *et al.*, *Sci. Transl. Med.* **5**, 208ra149 (2013).
34. C. Lagier-Tourenne *et al.*, *Proc. Natl. Acad. Sci. U.S.A.* **110**, E4530–E4539 (2013).

ACKNOWLEDGMENTS

We thank V. Funari for assistance with RNA sequencing, A. Cammack for assisting with patient tissue, and A. Koehne for assisting with pathology evaluation. This work was supported by NIH grants NS069669 (R.H.B), NS087351 (C.M.L), GM085796 (D.M.U.), NS078398 (T.M.M.), and UL1TR000124; the Robert and Louise Schwab family; the Cedars-Sinai ALS Research Fund (R.H.B.); and the Cedars-Sinai Board of Governors Regenerative Medicine Institute. T.M.M. has served on medical advisory boards for Ionis Pharmaceuticals and Biogen Idec. Mouse line F12 is available through the Jackson Repository, no. 27068, C57BL/6J-3110043021Rik<em5Lutzy>/J. RNA-seq data are located in the Gene Expression Omnibus, accession number GSE77681.

SUPPLEMENTARY MATERIALS

www.sciencemag.org/content/351/6279/1324/suppl/DC1
Materials and Methods
Supplementary Text
Figs. S1 to S11
Data Tables S1 and S2

20 December 2015; accepted 9 February 2016
10.1126/science.aaf1064

MUCOSAL IMMUNITY

Tuft cells, taste-chemosensory cells, orchestrate parasite type 2 immunity in the gut

Michael R. Howitt,[1] Sydney Lavoie,[1] Monia Michaud,[1] Arthur M. Blum,[2] Sara V. Tran,[3] Joel V. Weinstock,[2] Carey Ann Gallini,[1] Kevin Redding,[3] Robert F. Margolskee,[3] Lisa C. Osborne,[4]* David Artis,[4] Wendy S. Garrett[1,5,6]†

The intestinal epithelium forms an essential barrier between a host and its microbiota. Protozoa and helminths are members of the gut microbiota of mammals, including humans, yet the many ways that gut epithelial cells orchestrate responses to these eukaryotes remain unclear. Here we show that tuft cells, which are taste-chemosensory epithelial cells, accumulate during parasite colonization and infection. Disruption of chemosensory signaling through the loss of TRMP5 abrogates the expansion of tuft cells, goblet cells, eosinophils, and type 2 innate lymphoid cells during parasite colonization. Tuft cells are the primary source of the parasite-induced cytokine interleukin-25, which indirectly induces tuft cell expansion by promoting interleukin-13 production by innate lymphoid cells. Our results identify intestinal tuft cells as critical sentinels in the gut epithelium that promote type 2 immunity in response to intestinal parasites.

The mammalian gut microbiota is a collective of bacteria, archaea, viruses, fungi, and parasites that reside in the lumen and mucosal surface of the intestine. These microbes are sequestered from interior tissues by a single layer of epithelial cells lining the gut that acts as a barrier and sensor. Intestinal epithelial cells (IECs) express pattern recognition receptors that detect microbial components and thus are critical sensors for and orchestrators of mucosal immunity (*1*–*4*).

Beyond pattern recognition receptors, hosts monitor and respond to the microbiota via heterotrimeric guanine nucleotide–binding protein (G protein)–coupled receptors (GPCRs). For example, microbially produced short-chain fatty acids are sensed via GPR41 and GPR43 (*5*, *6*), and sinonasal epithelial cells can detect the pathogen *Pseudomonas aeruginosa* via a taste-chemosensory GPCR (*7*–*12*). Many taste-chemosensory GPCRs require the taste-specific G protein subunit gustducin and the cation channel TRPM5 to transduce their signals (*7*, *9*). The disruption of either gustducin or TRPM5 can perturb physiological responses to *P. aeruginosa* (*13*–*15*). In the gut, TRPM5 and other canonical taste-chemosensory components are predominantly expressed by an intestinal epithelial subset called tuft cells (*16*). Tuft cells, which are identified by the expression of doublecortin-like kinase 1 (DCLK1), comprise a minor fraction of small intestinal epithelial cells (*17*–*19*) and are putative quiescent stem cells (*20*). Although tuft cells express taste-chemosensory machinery, it is unknown whether tuft cells sense the gut microbiota by means of taste chemosensation or transduce signals to the mucosal immune system (*21*).

We began by evaluating the frequency of DCLK1$^+$ tuft cells in the distal small intestine of wild-type (WT) specific-pathogen-free mice that were bred in-house (BIH). We found markedly more intestinal DCLK1$^+$ tuft cells (7.2%) (Fig. 1A) than previous reports (0.4%) (*19*, *22*) and confirmed this discrepancy with an alternative tuft cell marker, GFI1B (fig. S1) (*23*). As interinstitutional differences in microbiota can contribute to substantial variation among mucosal immune cell populations (*24*), we compared tuft cell abundance in mice obtained from The Jackson Laboratory (JAX) with BIH mice. Similar to previous reports (*19*, *25*), tuft cells constituted 1.0% of the total IEC population of JAX mice (Fig. 1A). Feeding the cecal contents from BIH mice to JAX mice was sufficient to increase tuft cell populations to BIH levels (fig. S2), suggesting that transmissible components of the BIH microbiota may drive tuft cell expansion when introduced to JAX mice. In support of this idea, intestinal histology revealed numerous single-celled protozoa in BIH but not in JAX mice (Fig. 1B). To identify these protozoa, we purified and imaged them by means of scanning electron microscopy (SEM); we identified them as tritrichomonads (Fig. 1C) (*26*–*28*). Quantitative polymerase chain reaction (qPCR) confirmed that they were *Tritrichomonas muris* (Tm), a common but understudied member of the rodent microbiota (Fig. 1D).

To eradicate Tm from BIH mice, we added metronidazole (2.5 g/liter) to their drinking water for 1 week. This eliminated Tm and concomitantly reduced tuft cell abundance (fig. S3). Because this treatment does not exclude the possibility that other metronidazole-sensitive organisms may contribute to tuft cell expansion, we cultured Tm (*28*, *29*) and colonized unexposed mice. Tm colonization significantly elevated tuft cell numbers in

[1]Departments of Immunology and Infectious Diseases and Genetics and Complex Diseases, Harvard T. H. Chan School of Public Health, Boston, MA 02115, USA. [2]Division of Gastroenterology, Tufts Medical Center, Boston, MA 02111, USA. [3]Monell Chemical Senses Center, Philadelphia, PA 19104, USA. [4]Jill Roberts Institute for Research in Inflammatory Bowel Disease, Weill Cornell Medical College, Cornell University, New York, NY 10021, USA. [5]Broad Institute of Harvard and Massachusetts Institute of Technology, Cambridge, MA 02142, USA. [6]Department of Medical Oncology, Dana-Farber Cancer Institute, Boston, MA 02215, USA.
*Present address: Department of Microbiology and Immunology, University of British Columbia, Vancouver, British Columbia V6T 1Z3, Canada. **†Corresponding author. E-mail: wgarrett@hsph.harvard.edu**

Editor's Summary

Linking neurodegeneration and immune cells

The expansion of a repetitive DNA sequence in the C9orf72 gene is the major genetic cause of amyotrophic lateral sclerosis and frontotemporal dementia. Although the expansion decreases C9orf72 expression, most research has focused on the toxic RNA and protein products it creates in neurons. O'Rourke *et al.* found that C9orf72 unexpectedly plays a key role in innate immune cells. Loss of C9orf72 in mice led to macrophage and microglial dysfunction and age-related neuroinflammation. This raises the possibility of a "dual-effect" disease mechanism, in which toxic byproducts in neurons are combined with microglial dysfunction from decreased C9orf72 expression, together promoting neurodegeneration.

Science, this issue p. 1324